Published on 08 January 2025. Downloaded by BEIJING UNIVERSITY OF SCIENCE & TECHNOLOGY on 2/26/2025 2:41:04 PM.

Energy & Environmental Science

ROYAL SOCIETY OF CHEMISTRY

PAPER

View Article Online
View Journal | View Issue

Check for updates

Cite this: *Energy Environ. Sci.*, 2025, **18**, 1502

In situ construction of a hydrophobic channel interconnecting zincophilic planes on the Zn surface for enhanced stability of Zn metal anodes†

Miao Yu,[a] Jiawei Mu,[a] Lingfeng Wang,[a] Yuchao Niu,[a] Wenjie Si,[a] Jiale Li,[a] Xiaoyu Liu,[a] Tiantian Li,[a] Xiangcun Li,*[a] Wenji Zheng,[b] Yan Dai,[c] Xiaobin Jiang[a] and Gaohong He*[a]

Received 30th August 2024,
Accepted 19th December 2024

DOI: 10.1039/d4ee03945a

rsc.li/ees

The poor reversibility of Zn stripping/plating processes leads to unsatisfactory cycling stability of Zn anodes, limiting the practical application of aqueous zinc-ion batteries. Herein, sulfobutylether-β-cyclodextrin (SCD) was introduced into the electrolyte as a multi-functional additive. The zincophilic sulfonate groups were found to interact with Zn^{2+} to modulate the solvation structure, enhance adsorption and govern the adsorption configuration of SCD on the Zn surface. This specific adsorption configuration could *in situ* construct two planes on the Zn surface with progressively improved affinity to Zn^{2+}, which could drive the diffusion of Zn^{2+} through the hydrophobic toroidal inner channel, enable the uniform dispersion of Zn^{2+} flux and facilitate the de-solvation process. The synergistic promotional effect of the functional groups and specific structural features remarkably improved the stability of the Zn anode. With the addition of SCD, the Zn//Cu cell exhibited an extended cycle life of over 3000 cycles with an average CE exceeding 99.7%. The Zn//Zn symmetric cell also demonstrated superior cycling stability of over 3900 h at 2 mA cm^{-2}. The corresponding Zn//$NH_4V_4O_{10}$ full cells delivered a higher specific capacity and better cycling stability than cells using bare electrolytes. The assembled pouch cells were also stable for over 300 cycles, demonstrating the practical application potential of this electrolyte in high-performance AZIBs.

Broader context

Rechargeable aqueous zinc-ion batteries (AZIBs) are considered promising next-generation energy storage systems due to their high capacity, low cost and environmental benignity. However, the practical application of AZIBs is impeded by the instability of the zinc metal anode and the undesirable side reactions that occur during cycling. The development of effective electrolyte additives presents a promising and straightforward solution to address these challenges. Herein, sulfobutylether-β-cyclodextrin (SCD) is proposed as a multi-functional electrolyte additive that enhances the stability of the Zn surface and mitigates side reactions. Experimental characterizations and theoretical calculations demonstrate that the synergistic effects of the abundant zincophilic sulfonate groups and the unique structural features of SCD effectively stabilize the Zn anode. This leads to remarkable improvements in the electrochemical performance and cycling stability of the assembled cells. The cycling lifespans of both Zn//Cu asymmetric cells and Zn//Zn symmetric cells using the modified electrolyte are greatly improved. Furthermore, the Zn//$NH_4V_4O_{10}$ full cells exhibit higher specific capacity and better cycling stability than the cells using bare electrolytes. This research offers valuable insights for the development of advanced electrolytes for AZIBs.

[a] *State Key Laboratory of Fine Chemicals, Frontier Science Center for Smart Materials, School of Chemical Engineering, Dalian University of Technology, No. 2 Linggong Road, Ganjingzi District, Dalian City, 116024, Liaoning Province, P. R. China. E-mail: lixiangcun@dlut.edu.cn, hgaohong@dlut.edu.cn*

[b] *State Key Laboratory of Fine Chemicals, School of Chemical Engineering, Ocean and Life Sciences, Dalian University of Technology, No. 2 Dagong Road, Liaodong Bay New District, Panjin City, 124221, Liaoning Province, P. R. China*

[c] *Panjin Institute of Industrial Technology, Liaoning Key Laboratory of Chemical Additive Synthesis and Separation, No. 2 Dagong Road, Liaodong Bay New District, Panjin City, 124221, Liaoning Province, P. R. China*

† Electronic supplementary information (ESI) available. See DOI: https://doi.org/10.1039/d4ee03945a

1. Introduction

Rechargeable aqueous zinc-ion batteries (AZIBs) are considered a promising next-generation technology for large-scale energy storage and conversion applications due to the high abundance of Zn metal, low cost, high theoretical capacity (820 mA h g^{-1} and 5855 mA h cm^{-3}), inherent safety, and environmental benignity. However, AZIBs not only inherit the advantages of Zn metal but also suffer from the associated challenges,

This journal is © The Royal Society of Chemistry 2025

Published on 08 January 2025. Downloaded by BEIJING UNIVERSITY OF SCIENCE & TECHNOLOGY on 2/26/2025 2:41:04 PM.

including notorious dendrite growth, corrosion, byproduct formation, and the inevitable hydrogen evolution reaction (HER). These problems severely restrict the cycling stability and lifespan of AZIBs and are well-recognized as the main obstacles hindering the commercialization of AZIBs.[1–3] Overcoming these issues has attracted massive attention, leading to the development of new strategies focused on modifying the anode, separator, and electrolyte.[4–8] Among these approaches, introducing functional additives into the electrolyte can simultaneously optimize the diffusion and deposition behaviors of Zn^{2+} by regulating its solvation structure and modulating the electrolyte/anode interface. Moreover, electrolyte engineering is a straightforward and effective method that can be easily adopted in practical production and application processes.[9,10]

Various kinds of electrolyte additives, such as metal salts, amino acids, organic solvents, and chelating ligands, have been reported to stabilize the Zn surface by facilitating the de-solvation process of hydrated Zn^{2+}, suppressing the HER and side reactions, or inhibiting the formation and growth of dendrites. Meanwhile, various mechanisms have been proposed, including interactions with Zn^{2+} to regulate the solvation shell structure or with the anode surface to modulate the electric double layer (EDL) and electric field and induce preferential orientation of Zn deposition. Since these issues are critical and directly impact the stability of the Zn anode and the lifespan of the assembled batteries, the ideal electrolyte additives should be capable of providing multiple synergistic effects. Small molecules mainly impact the electrochemical performance with functional groups like hydroxyl,[11–13] carbonyl,[14] carboxyl,[12] and sulfonate,[15] but their relatively simple structures restrict these additives making multiple contributions. Supramolecule materials are composed of small organic molecules with certain structures and have shown great potential in improving the stability of the Zn surface by effectively through the advantages offered by the abundant functional groups and specific structures.[16–22] However, there are currently no supramolecule additives that have been reported to stabilize Zn anodes by simultaneously combining the advantages of both the functional groups and structural features. Hence, the understanding and development of supramolecule additives need to be enhanced, which could be expected to be an effective means to improve the electrochemical performance.

Herein, we propose the utilization of sulfobutylether-β-cyclodextrin (SCD) as an electrolyte additive to stabilize the Zn metal anode. SCD molecules not only contain abundant hydroxyl groups, like other cyclodextrin (CD) molecules, but also contain seven sulfonate groups with strong zincophilicity in the sulfobutylether chains. These sulfonate groups endow SCD with the ability to modulate the solvation structure of Zn^{2+}, which other CDs do not have. Simultaneously, these sulfonate groups also increase the adsorption strength, and further govern the adsorption configuration of toroidal SCD molecules on the Zn surface. The adsorbed SCD molecules *in situ* construct two planes with a progressively improved affinity to Zn^{2+}, which can drive the diffusion and uniform dispersion of Zn^{2+}, while the hydrophobic interior can further repel H_2O molecules and facilitate the de-solvation process when Zn^{2+} ions pass though the toroidal channel. Benefiting from the multiple promotional effect originating from the abundant functional groups and specific structural features, the stability of Zn anodes in the modified electrolyte can be significantly improved. A Zn//Cu asymmetric cell exhibited a long cycle life of over 3000 cycles (2 mA cm^{-2}, 1 mA h cm^{-2}) with an average CE of 99.7%. Zn//Zn symmetric cells could steadily work for 3900 h (2 mA cm^{-2}, 1 mA h cm^{-2}), and also showed excellent performance in the discharge (5 mA cm^{-2}, 51.3% DOD, ~500 h) and cumulative plating capacity tests (10 mA cm^{-2}, 3 mA h cm^{-2}, 5.175 A h cm^{-2}). The corresponding Zn//$NH_4V_4O_{10}$ full cells also delivered higher specific capacity and better cycling stability than the cells using bare electrolytes. This study provides a novel perspective for designing electrolyte additives for high-performance AZIBs.

2. Results and discussion

To investigate the effect of SCD on the properties of bare electrolytes (2 M $ZnSO_4$, ZS), Fourier transform infrared spectroscopy (FTIR), Raman spectroscopy, and nuclear magnetic resonance (NMR) were utilized. With the increase in SCD concentration, the characteristic peaks of the C–H bonds between 2800–3000 cm^{-1} gradually appeared (Fig. 1(a)). Meanwhile, the O–H stretching vibration in H_2O between 3200–3250 cm^{-1} showed a blue-shift, which suggested that SCD could weaken the hydrogen bond network between H_2O molecules.[23] Additionally, the emergence of a new peak assigned to the O–H stretching vibration in $-SO_3-H$ at around 3650 cm^{-1} further confirmed the participation of SCD in the hydrogen bond network in the electrolyte.[24] The change in the solvation structure of Zn^{2+} in different electrolytes was investigated by analyzing the ν-SO_4^{2-} band in the Raman spectra (Fig. 1(b) and Fig. S1, ESI†). The ν-SO_4^{2-} band could be divided into two regions and assigned to two forms of ion pair species, namely the solvent separated ion pair (SSIP, $[Zn^{2+}(H_2O)_6SO_4^{2-}]$) and contact ion pair (CIP, $[Zn^{2+}(H_2O)_5OSO_3^{2-}]$).[25] In ZS electrolyte, the SSIP and CIP species accounted for 64.1% and 35.9%, respectively, according to the ratio of the peak areas. With the increase in SCD concentration from 5 mM to 20 mM, the ratio of CIP progressively decreased to 27.3% and the ratio of SSIP increased to 72.7%. This indicates that the interaction between Zn^{2+} and SO_4^{2-} was weakened and thus it was more difficult for SO_4^{2-} to participate in the solvation shell of Zn^{2+}, which suggests that the coordination environment of Zn^{2+} could be regulated by the presence of SCD due to the strong affinity of the $-SO_3^-$ and –OH groups toward Zn^{2+}.[26,27] The ^2H peak in the NMR of pure D_2O was located at 4.702 ppm (Fig. 1(c)). After adding 2 M $ZnSO_4$, the ^2H peak notably shifted to 4.726 ppm, which was attributed to the decrease in electron density around D_2O and the weakened proton shielding due to the coordination between Zn^{2+} and D_2O. As the concentration of SCD increased from 0 to 20 mM, the ^2H peak gradually shifted to 4.723 ppm. This suggested that the interaction between Zn^{2+} and SCD was stronger than that

Published on 08 January 2025. Downloaded by BEIJING UNIVERSITY OF SCIENCE & TECHNOLOGY on 2/26/2025 2:41:04 PM.

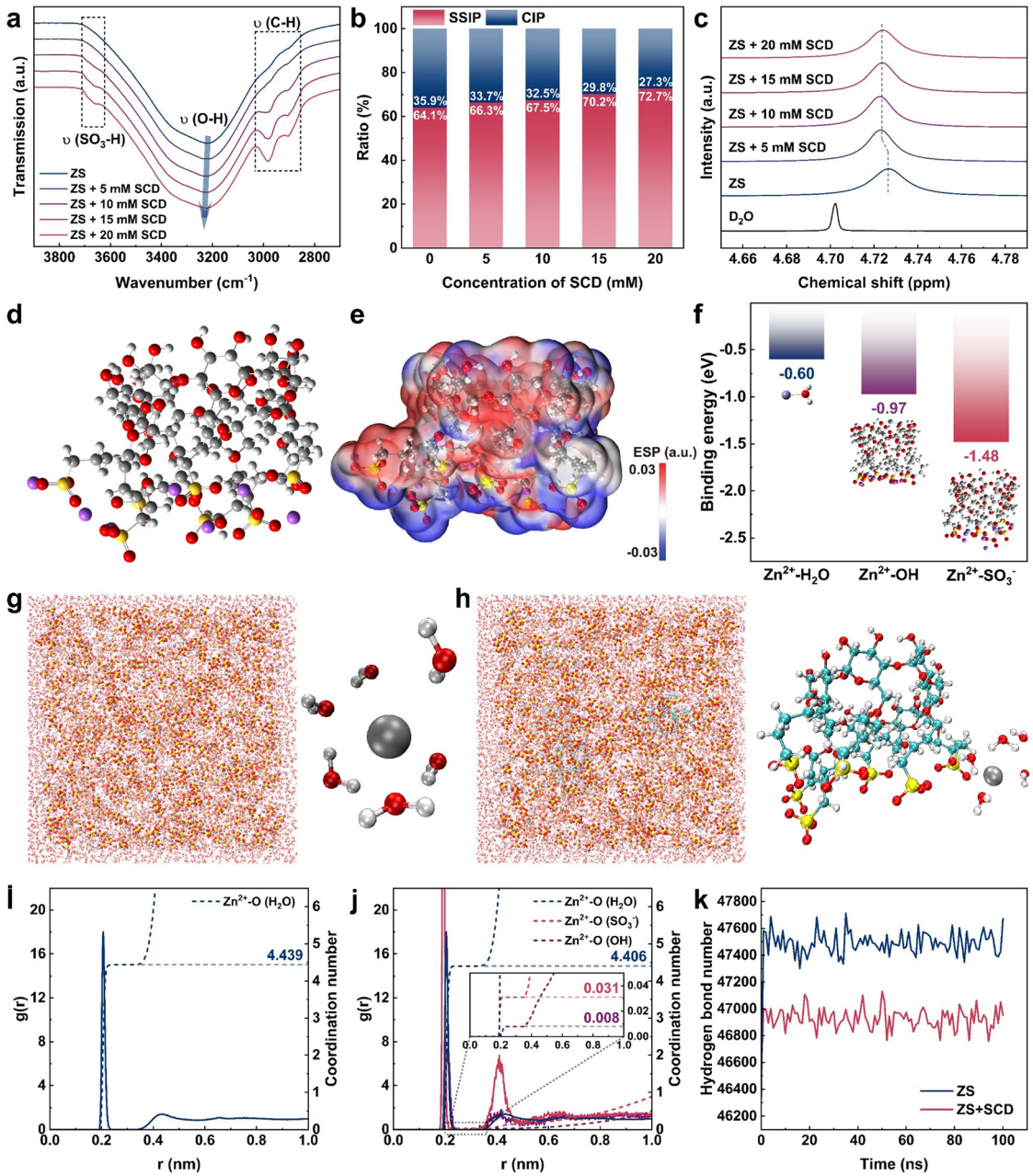

Fig. 1 (a) FTIR spectra of different electrolytes. (b) SSIP and CIP ratios of different electrolytes from the Raman spectra. (c) NMR spectra of the ^{2}H nuclei for different electrolytes. (d) and (e) Molecule structure and ESP mapping of SCD. (f) Binding energies of Zn^{2+} with H_2O and SCD. (g) and (h) 3D snapshots of ZS and ZS + SCD electrolytes obtained from MD simulations, showing the corresponding Zn^{2+} solvation structures. (i) and (j) RDFs and corresponding ACNs of Zn^{2+} solvation structures. (k) Hydrogen bond numbers of ZS and ZS + SCD electrolytes in a unit volume.

between Zn^{2+} and water molecules, thus some water molecules were replaced and released from the Zn^{2+} solvation structure.[11]

Density functional theory (DFT) and molecular dynamics (MD) simulations were further employed to reveal the effect of SCD on the Zn^{2+} solvation structure. Fig. 1(d), (e) and Fig. S2 (ESI†) illustrate the electrostatic potential mappings of the SCD molecule. The abundant $-SO_3^-$ and –OH groups provide multiple regions with low electron density, which favors the adsorption of Zn^{2+}. The binding energies of Zn^{2+} on the $-SO_3^-$ and –OH groups were calculated to be −1.48 and −0.97 eV, respectively, which are both much higher than that of Zn^{2+} on a H_2O molecule (−0.60 eV) (Fig. 1(f)). The stronger interaction between these functional groups and Zn^{2+} suggests that SCD would preferentially enter into the Zn^{2+} solvation structure.[11,28] A detailed analysis of the Zn^{2+} solvation structures in ZS and ZS + SCD electrolytes was performed with MD simulations, and the representative Zn^{2+} coordination structures are illustrated in Fig. 1(g) and (h). Compared to that in the ZS electrolyte, the 3D snapshot of the ZS + SCD electrolyte illustrates that the SCD molecule could indeed replace the H_2O

 This journal is © The Royal Society of Chemistry 2025

Published on 08 January 2025. Downloaded by BEIJING UNIVERSITY OF SCIENCE & TECHNOLOGY on 2/26/2025 2:41:04 PM.

molecule, participate in the solvation shell, and coordinate with Zn^{2+} *via* the $-SO_3^-$ group. The radial distribution functions (RDFs) and the average coordination numbers (ACNs) of Zn^{2+}–H_2O and Zn^{2+}–SCD are shown in Fig. 1(i) and (j). In the ZS electrolyte, the peak representing the Zn^{2+}–O (H_2O) coordination appeared at ~2.0 Å with an ACN of 4.439, demonstrating that Zn^{2+} ions were mainly coordinated with H_2O molecules in the ZS electrolyte. With the addition of SCD, the ACN of Zn^{2+}–O (H_2O) decreased to 4.406, while the ACNs of Zn^{2+} with the functional groups in SCD, Zn^{2+}–O (SO_3^-), and Zn^{2+}–O (OH) are 0.031 and 0.008, respectively, which further evidenced the change of Zn^{2+} coordination structure due to the favorable electrostatic interaction between Zn^{2+} and the functional groups in SCD. The higher ACN of Zn^{2+}–O (SO_3^-) over Zn^{2+}–O (OH) was determined by the stronger interaction between Zn^{2+} and SO_3^-, as revealed in the DFT calculation results. Additionally, the statistical analysis revealed that the number of hydrogen bonds in the ZS + SCD electrolyte was slightly lower than that in the ZS electrolyte (Fig. 1(k)). This suggests that the addition of SCD could disrupt the hydrogen bond network between H_2O molecules to some extent, which was in accordance with the FTIR results. This disruption might slightly reduce the ratio of active H_2O molecules, potentially offering some benefit in suppressing the HER side reaction.[11,25]

The energy levels of the highest occupied molecular orbital (HOMO) and the lowest unoccupied molecular orbital (LUMO) for SCD and H_2O were calculated (Fig. 2(a)). The HOMO energy level of SCD was higher than that of H_2O, revealing that the electrons from SCD were more easily transferred to the Zn surface after adsorption. Meanwhile, the LUMO energy level of SCD was lower than that of H_2O, suggesting that SCD molecules were more likely to receive electrons than H_2O, thus preferentially reducing the decomposition of H_2O and suppressing the HER side reaction.[11,13,15,26] DFT simulation was then applied to evaluate the adsorption properties of SCD on the Zn surface, and considering the large molecule size of SCD, the unit structure (sodium sulfobutylether-glucose, NaSG) was selected as the representative (Fig. 2(b) and Fig. S4, ESI†). The adsorption energy of H_2O on the Zn(002) surface was only −0.32 eV, while the adsorption energy of SG^- anion was calculated to be −4.28 eV. The corresponding differential charge density distribution illustrated a stronger electron cloud overlap between

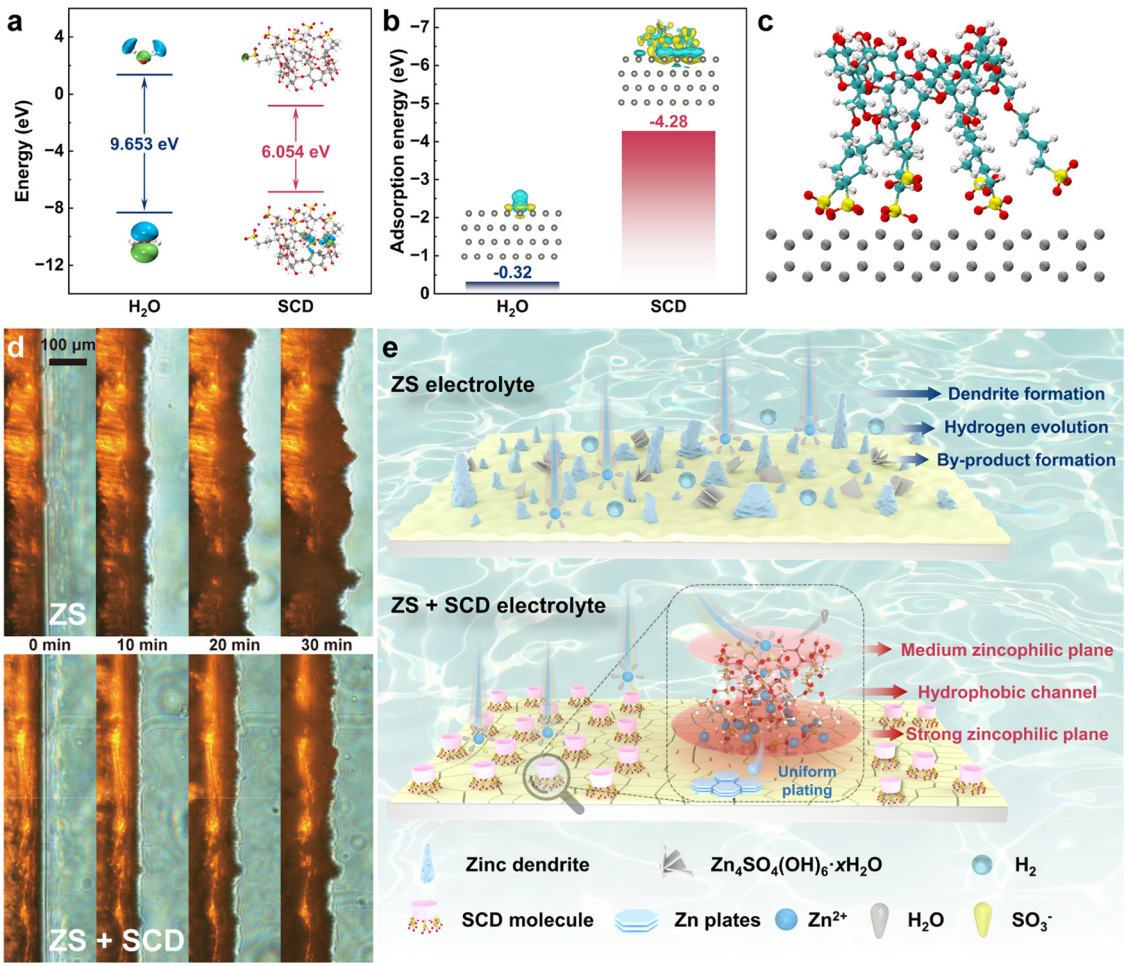

Fig. 2 (a) HOMO and LUMO isosurfaces of H_2O and SCD. (b) Comparison of adsorption energies for H_2O and SCD units on the Zn(002) plane; insets show the corresponding adsorbed models and differential charge densities. (c) Adsorption configuration of SCD on the Zn surface. (d) *In situ* optical microscopy images of Zn deposition in ZS and ZS + SCD electrolytes. (e) Schematic of Zn deposition in ZS and ZS + SCD electrolytes.

Published on 08 January 2025. Downloaded by BEIJING UNIVERSITY OF SCIENCE & TECHNOLOGY on 2/26/2025 2:41:04 PM.

the O in $-SO_3^-$ and –OH and Zn metal than that between the H_2O and Zn metal. The shortened Zn–O bond length (2.10 Å for $Zn-SO_3^-$ and 2.21 Å for Zn–OH *vs.* 2.44 Å for $Zn-H_2O$) further evidenced the stronger interaction between SG^- and Zn.[29] It is worth mentioning that due to the more abundant zincophilic groups in the SCD molecule, the interaction between the SCD and Zn surface could be predicted to be even stronger. Therefore, in ZS + SCD electrolyte, the SCD molecule can repulse H_2O and preferably adsorb on the Zn surface, which can modulate the EDL on the Zn surface and suppress the HER side reaction.[30] The preferential adsorption of SCD on Zn surface was further evidenced by MD simulation, and it could be observed that the adsorbed SCD molecules tended to exhibit a specific configuration with the SO_3^- groups attached on the Zn surface due to the stronger interaction (Fig. 2(c) and Fig. S5, ESI†). The X-ray photoelectron spectra (XPS) of O 1s and S 2p (Fig. S6 and S7, ESI†) further supported this adsorption behavior. While the O 1s spectra showed minimal changes between SCD powder and the SCD-treated Zn plate, the S 2p spectra revealed a prominent shift to higher binding energy. This shift occurred because the O atoms in the sulfonate groups interact with Zn, reducing the electron density on the S atoms and increasing the S 2p binding energy, indicating that all the sulfonate groups were directly involved in the interaction. The MD simulation further revealed that the SO_3^- groups contributed ~90% of the total interaction energy between SCD molecule and Zn surface (Fig. S8, ESI†). Consequently, the distinctive adsorption configuration forms a strong zincophilic plane on the Zn surface, with the hydroxyl groups creating a medium zincophilic plane on the opposite side of the adsorbed Zn surface. This distinctive molecule structure and adsorption configuration can *in situ* construct two planes on the Zn surface with a progressively improved affinity to Zn^{2+}, which can drive the diffusion of Zn^{2+} through the toroidal channel, disperse the Zn^{2+} flux, and finally realize uniform deposition on Zn surface facilitated by the electrostatic and electric field force.[31] Additionally, the hydrophobic nature of the inner cavity in CD structure can facilitate the de-solvation of hydrated Zn^{2+}, so the side reactions can be suppressed simultaneously.[16,21] Thus, SCD is expected to be an effective electrolyte additive to improve the stability of Zn anodes and the overall performance of AZIBs.

To investigate the effect of the SCD concentration additive on the electrolyte, various measurements were performed to evaluate the physicochemical properties of these electrolytes. With the increase in the concentration of SCD from 0 to 20 mM, the pH value of the electrolytes was slightly decreased from 4.34 to 4.16 (Fig. S9, ESI†). Compared to other reported electrolyte additives, the effect of SCD on the pH value was trivial, thus the possible change in the corrosion behavior of Zn anodes and the formation of $Zn_4SO_4(OH)_6{\cdot}xH_2O$ by-products could hardly be attributed to the change of the pH environment. The viscosity of different electrolytes was also measured since the fluidity of the electrolyte directly influences the ion-transport behavior. When the concentration of SCD was lower than 10 mM, the addition of SCD could lower the viscosity of the electrolyte (Fig. S10, ESI†). This was probably because the SCD could interact with H_2O molecules, disrupt the orderly structure, and reduce the frictional forces between molecules. However, as the concentration of SCD increases, the self-interaction between SCD molecules might assemble into network structures and result in the increased viscosity. The ionic conductivity of different electrolytes was measured (Fig. S11, ESI†). Generally, the addition of SCD had a negative effect on ion transport, which suggested that the strong interaction between SCD and Zn^{2+} might hamper ionic transfer to some extent. However, the decrease in ionic conductivity was trivial when the concentration of SCD was below 10 mM (67.5 *vs.* 65.8 mS cm^{-1}), which probably benefited from the improved fluidity of the electrolyte.[32] Thus, after comprehensive consideration of the effect of the SCD additive on the above properties of the electrolyte, 10 mM was selected as the optimal concentration for further investigation of its performance in stabilizing the Zn anode under different conditions.

To investigate the interfacial property between the Zn surface and the electrolytes, Zn plates were further immersed in ZS and ZS + SCD electrolytes for 3 days and then examined by SEM and XRD. The SEM images illustrated that in the ZS electrolyte, abundant big flakes could be observed on the Zn surface, while the surface remained relatively flat in the ZS + SCD electrolyte (Fig. S12, ESI†). Since the concentration of SCD was relatively low, the formation of the by-product $Zn_4SO_4(OH)_6{\cdot}4H_2O$ was not fully eliminated, but the intensity of the corresponding peak was still significantly lower (Fig. S13, ESI†).[33] The abundant hydroxyl and sulfonate groups in SCD can also benefit the wettability of ZS + SCD electrolyte on Zn surface to some extent, as revealed by a slightly decreased contact angle from 89.2° to 85.0° (Fig. S14, ESI†).[32,34] The plating processes in different electrolytes on the Zn surface were recorded by *in situ* optical microscopy at a current density of 5 mA cm^{-2} (Fig. 2(d)).[26,35] Obvious protrusions could already be observed on the Zn surface after only 10 min in the ZS electrolyte, and the severe dendrite growth almost doubled the apparent thickness of the Zn plate after 30 min. In contrast, the protrusions were much smaller under the same conditions and the Zn plate maintained a relatively flat and compact surface in the ZS + SCD electrolyte. This intuitive comparison demonstrates the effectiveness of SCD in stabilizing the Zn anode due to its distinctive molecular structure and adsorption configuration. Combined with previous DFT and MD results, the proposed mechanism is elaborately illustrated in Fig. 2(e).

The effect of SCD on inhibiting the HER on the Zn surface was investigated with linear sweep voltammetry (LSV). The LSV curves showed that, with the addition of SCD, the potential increased from −1.818 V to −1.883 V (*vs.* Ag/AgCl) at −10 mA cm^{-2}, while the current density was kept smaller throughout, which indicates that the presence of SCD could effectively inhibit the hydrogen evolution side reaction (Fig. 3(a)).[36] Meanwhile, the electrochemical stability window (ESW) of the ZS and ZS + SCD electrolytes further showed that the oxidative stability was not affected with the addition of SCD (Fig. S15, ESI†). Linear polarization tests were further conducted to evaluate the anti-corrosion behavior of these two electrolytes. As revealed in the Tafel plots, the addition of SCD could simultaneously increase the corrosion potential from

 This journal is © The Royal Society of Chemistry 2025

Published on 08 January 2025. Downloaded by BEIJING UNIVERSITY OF SCIENCE & TECHNOLOGY on 2/26/2025 2:41:04 PM.

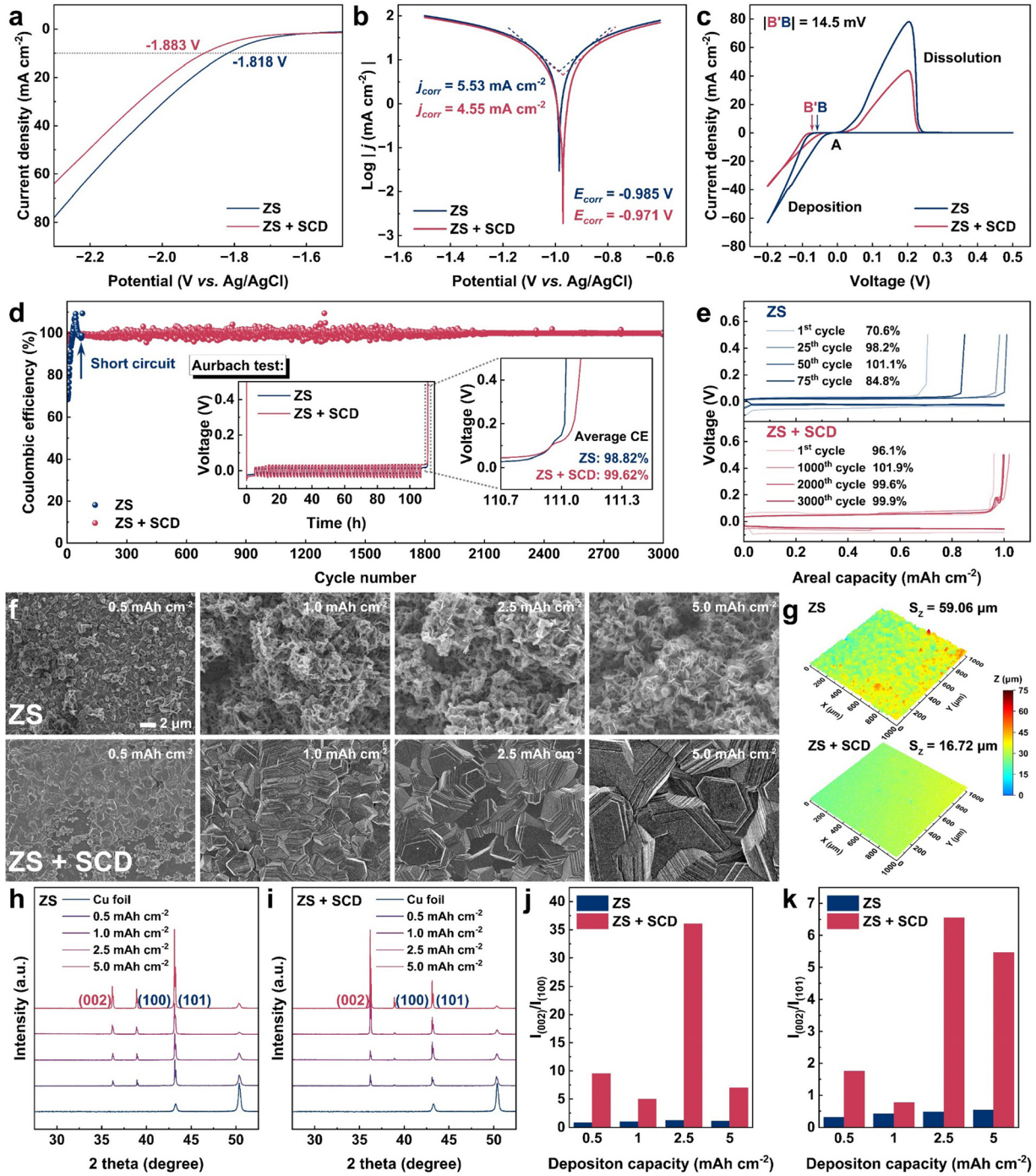

Fig. 3 (a) Linear sweep voltammetry profiles and (b) linear polarization curves of the Zn anode in ZS and ZS + SCD electrolytes using a three-electrode system. (c) CV curves of Zn plating/stripping in Zn//Cu asymmetric cells. (d) Coulombic efficiency (CE) of Zn//Cu cells in ZS and ZS + SCD electrolytes at 2 mA cm^{-2} with a capacity of 1 mA h cm^{-2}; insets: voltage profiles from Aurbach tests, and (e) corresponding voltage profiles at various cycles. (f) Surface morphologies of deposited Zn on a Cu substrate in ZS and ZS + SCD electrolytes at 5 mA cm^{-2} with various areal capacities, and corresponding (g) laser confocal microscopy images, (h), (i) XRD patterns and (j), (k) diffraction peak intensity ratios.

−0.985 V to −0.971 V (*vs.* Ag/AgCl), and lower the corrosion current density from 5.53 mA cm^{-2} to 4.55 mA cm^{-2}, thereby suggesting that SCD could potentially protect the Zn surface from being corroded (Fig. 3(b)).[15,35] The CV curve of the Zn//Cu asymmetric cell was obtained to elucidate the effect of SCD on the Zn^{2+}-deposition behavior (Fig. 3(c)). The nucleation overpotential in the ZS + SCD electrolyte was slightly higher than that in the ZS electrolyte (|B′B| = 14.5 mV), and the redox peak was also weaker. This indicated that the preferential adsorption of SCD could cause steric hindrance and reduce the nucleation sites on the Zn surface. Furthermore, the relationship between the grain radius of Zn (r) and the nucleation overpotential (η) followed

Published on 08 January 2025. Downloaded by BEIJING UNIVERSITY OF SCIENCE & TECHNOLOGY on 2/26/2025 2:41:04 PM.

the equation:[21,25,29,30,37]

$$r = 2\frac{\gamma V_m}{F|\eta|}$$

where γ is the surface energy of the electrode/electrolyte interface, V_m is the molar volume of Zn, and F is the Faraday constant. According to the contact angle results, SCD could reduce the Zn/electrolyte interface energy, while the increased nucleation overpotential could further benefit the formation of smaller nuclei and suppress dendrite growth.

Zn plating/stripping tests were further performed using asymmetric Zn//Cu cells to investigate the reversibility of the Zn anode in different electrolytes at 2 mA cm^{-2} and 1 mA h cm^{-2} with a cut-off voltage of 0.5 V. It was found that the addition of SCD could improve the cycle life and the average Coulombic efficiency (CE), with the electrolyte containing 10 mM SCD exhibiting the optimal performance, which was in line with previous expectations (Fig. 3(d) and Fig. S16, ESI†). The Zn//Cu cell with the ZS electrolyte exhibited a low initial CE of only 70.6% and suffered from poor stability and severe fluctuation, and encountered a short-circuit after only 70 cycles. While with the presence of SCD, the initial CE was increased to 96.1%, and after experiencing a fluctuation induced by the surface reconstruction, the cell finally exhibited a long cycle life of over 3000 cycles with relatively stable voltage profiles (Fig. 3(e)). The higher average CE of the Zn//Cu cell with ZS + SCD (99.62% *vs.* 98.82%) determined by the Aurbach tests further demonstrated the contribution of SCD to the stability of Zn plating/stripping processes. The peak that appeared at 0.1 to 0.2 V indicated that additional energy was needed to realize the full stripping of Zn. This was probably due to the strong affinity between SCD and the deposited Zn, as evidenced by the synchronized reduction in the intensity of the Zn 2p and S 2p peaks in the XPS spectra after this peak (Fig. S17, ESI†). Additionally, the addition of SCD could modulate the deposition morphology of Zn on a Cu substrate. SEM images of the Cu surface after Zn deposition with capacities of 0.5, 1.0, 2.5, and 5.0 mA h cm^{-2}, respectively, at a current density of 5.0 mA cm^{-2} were recorded (Fig. 3(f) and Fig. S18, S19, ESI†). It was observed Zn^{2+} tended to aggregate on the Cu surface and formed irregular and loose dendrites with unoriented flakes in the ZS electrolyte. While with the presence of SCD, Zn^{2+} was uniformly deposited and finally grew into large, flat, and tightly compacted flakes with a lower average roughness, as evidenced by the confocal laser scanning microscopy (CLMS) images (Fig. 3(g)). These flat flakes corresponded to the typical morphology of the (002) plane of Zn,[38,39] which could be further confirmed by the stronger intensity of the peak corresponding to the (002) plane and the larger intensity ratio of $I_{(002)}/I_{(100)}$ and $I_{(002)}/I_{(101)}$ in the ZS + SCD electrolyte according to the XRD patterns of the deposited Cu plate (Fig. 3(h)–(k)).[40] Furthermore, the thickness of the deposited Cu plates was measured using a digital micrometer, and the SEM images of the cross-sections intuitively illustrated that the Zn layer in ZS + SCD was much thinner and more compact, which suggests that SCD could effectively inhibit the formation and growth of Zn dendrites (Fig. S20, ESI†).

The Zn^{2+} transference number increased from 0.38 in the ZS electrolyte to 0.60 in the ZS + SCD electrolyte, which demonstrated that the addition of SCD enhanced the Zn^{2+}-diffusion kinetics, and the fast diffusion of Zn^{2+} could alleviate the concentration gradient near the Zn surface and thus suppress the dendrite growth (Fig. 4(a) and Fig. S21, ESI†).[26] The chronoamperometric (CA) method was used to analyze the nucleation and growth behavior of Zn^{2+} with different electrolytes under a constant overpotential of −150 mV (Fig. 4(b)). The current density in the ZS electrolyte continuously increased, which indicated that the Zn^{2+} preferably underwent lateral in-plane 2D diffusion on the Zn surface. This in-plane diffusion would induce the aggregation of Zn^{2+} and result in the generation of unevenly distributed nuclei and dendrite formation. Contrarily, the current density in the ZS + SCD electrolyte was only increased in the first 50 s and then maintained a steady value, demonstrating the stable directional 3D diffusion behavior of Zn^{2+}, which is beneficial to realizing uniform plating.[35] This is because the adsorbed SCD on the Zn surface provided abundant anchoring sites for Zn^{2+} and simultaneously restricted the lateral 2D diffusion. To investigate the adsorption behavior of SCD on the Zn surface, cyclic voltammetry tests at different scan rates were performed to measure the EDL capacitance of Zn//Zn symmetric cells using ZS and ZS + SCD electrolytes (Fig. S22, ESI†). It was found that the EDL capacitance of the Zn surface significantly decreased from 161.55 μF cm^{-2} in the ZS electrolyte to 91.79 μF cm^{-2} with the presence of SCD, which indicates that the adsorption of SCD increased the thickness of the Zn^{2+}-diffusion layer, as evidenced in the DFT and MD simulation results (Fig. 4(c)).[15,25,34,40]

The rate performance of the Zn//Zn symmetric cells in two electrolytes was evaluated at a fixed capacity of 1 mA h cm^{-2} with the current density varying from 0.5 to 10 mA cm^{-2} (Fig. 4(d)). Both cells kept stable at each current density, but when the current density returned to 0.5 mA cm^{-2}, the voltage hysteresis of the cell with the ZS electrolyte gradually increased and encountered a short-circuit after 220 h. On the contrary, the voltage hysteresis of the cell with the ZS + SCD electrolyte stayed unchanged for 680 h under the same conditions, which revealed the effective protection of SCD on the Zn surface against fast Zn^{2+}-plating and -stripping processes. Based on the voltage hysteresis values under different current densities, the exchange current density was calculated by linearly correlating the overpotentials with the corresponding current densities (Fig. 4(e)). The lower exchange current density of the ZS + SCD electrolyte (3.32 mA cm^{-2}) compared to that of the ZS electrolyte (3.50 mA cm^{-2}) suggested that the addition of SCD could promote the uniform distribution of the local current density and reduce the distortion of the surface electric field, which could lead to a dendrite-free electrodeposition of Zn.[41,42] The activation energy (E_a) of the Zn^{2+} de-solvation process could be employed to evaluate the kinetics of Zn^{2+} deposition, which was obtained from the impedance change of the Zn//Zn symmetric cell under different temperatures. The electrochemical impedance spectra (EIS) of the symmetric cells with and without SCD from 298 to 338 K are shown in Fig. S23 (ESI†), and the E_a values were calculated according to the Arrhenius equation.

 This journal is © The Royal Society of Chemistry 2025

Published on 08 January 2025. Downloaded by BEIJING UNIVERSITY OF SCIENCE & TECHNOLOGY on 2/26/2025 2:41:04 PM.

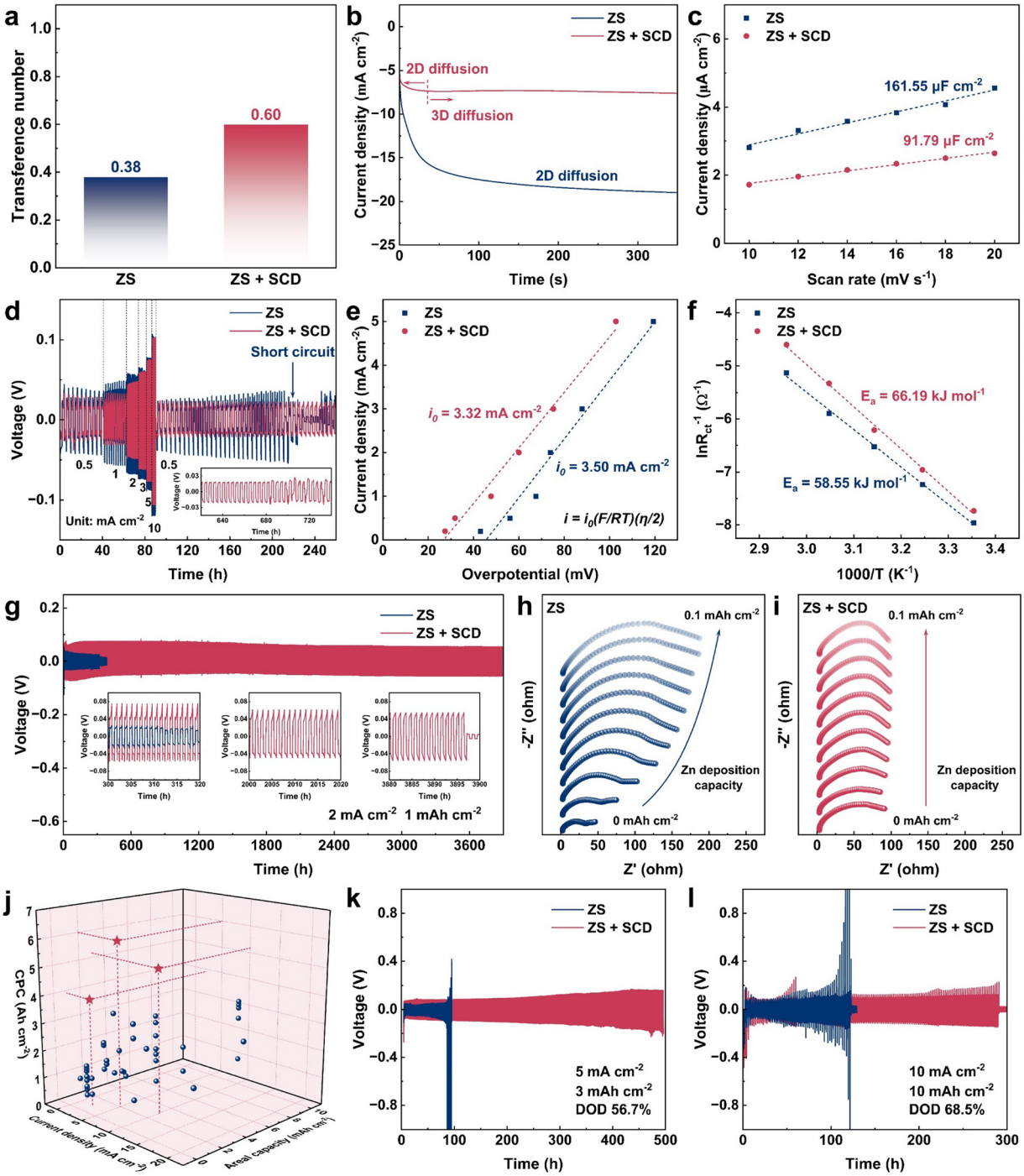

Fig. 4 (a) Calculated Zn^{2+} transference number in ZS and ZS + SCD electrolytes. (b) Chronoamperometry curves of the Zn^{2+} plating process in ZS and ZS + SCD electrolytes with an overpotential of −150 mV. (c) Plots of capacitive currents *versus* scan rate for calculating the EDL capacitances of the Zn surface in ZS and ZS + SCD electrolytes. (d) Rate performance at various current densities with a capacity of 1 mA h cm^{-2} and (e) exchange current densities of Zn//Zn symmetric cells using ZS and ZS + SCD electrolytes. (f) Arrhenius curves and corresponding de-solvation activation energies. (g) Cycling performance of Zn//Zn symmetric cells using ZS and ZS + SCD electrolytes at 2 mA cm^{-2} with a capacity of 1 mA h cm^{-2}. (h) and (i) *In situ* electrochemical impedance spectra of Zn//Zn symmetric cells using ZS and ZS + SCD electrolytes. (j) Comparison of the current density, areal capacity and cumulative plating capacity of Zn//Zn symmetric cells using ZS + SCD electrolytes with other reported literature values. Cycling performance of Zn//Zn symmetric cells using ZS and ZS + SCD electrolytes at (k) 5 mA cm^{-2}, 3 mA h cm^{-2} under 56.7% DOD, and (l) 10 mA cm^{-2}, 10 mA h cm^{-2} under 68.5% DOD.

With the addition of SCD, the E_a value exhibited an increase from 58.55 to 66.19 kJ mol^{-1} (Fig. 4(f)). This further verified that the Zn^{2+}-deposition rate was reduced by SCD, which is beneficial for the generation of uniform Zn nucleation and can contribute to improving the cycle stability of the Zn//Zn symmetric cell.[23,25]

Published on 08 January 2025. Downloaded by BEIJING UNIVERSITY OF SCIENCE & TECHNOLOGY on 2/26/2025 2:41:04 PM.

When the current density was set as 2 mA cm^{-2} with a capacity density of 1 mA h cm^{-2}, the cell with the ZS electrolyte encountered a short-circuit after 300 h. The cell with the electrolyte containing 10 mM SCD still delivered superior cycling stability over other electrolytes, exhibiting a stable voltage profile for 3900 h (Fig. 4(g) and Fig. S24, ESI†). The voltage hysteresis increased with the addition of SCD, which was in accordance with the lower exchange current density. The prolonged cycling stability demonstrated that the optimized Zn^{2+}-deposition rate had a decisive impact on inhibiting the side reactions and dendrite-growth processes. The SEM images of the Zn surface from the symmetric cells after 100 cycles at 2 mA cm^{-2} and 1 mA h cm^{-2} illustrated that the Zn deposition in the ZS + SCD electrolyte was more uniform and flatter, and the XRD patterns also indicated that the formation of by-products was also effectively inhibited by SCD (Fig. S25–S27, ESI†). The adsorption of SCD on the Zn surface induced the increase in the charge-transfer resistance (R_{ct}) of the symmetric cell, while the *in situ* EIS measurements revealed that the R_{ct} kept stable during the deposition of Zn, benefiting from the protective effect of SCD on the Zn surface. Conversely, the R_{ct} of the cell with the ZS electrolyte gradually increased due to the formation and accumulation of by-products (Fig. S28, ESI† and Fig. 4(h), (i)).[15,23,30,43] Additionally, a significant improvement was also obtained with the addition of SCD when the current densities and capacities were further elevated to 5 mA cm^{-2} and 2 mA h cm^{-2} (Fig. S29, ESI†). Even under the more challenging conditions of 10 mA cm^{-2} and 3 mA h cm^{-2}, the Zn//Zn symmetric cell using the ZS + SCD electrolyte still exhibited excellent cycling stability for over 1035 h, corresponding to an extraordinarily high cumulative plating capacity (CPC) of 5.175 A h cm^{-2} (Fig. S30, ESI†). The CPC values of these cells were also prominent compared to previously reported values (Fig. 4(j) and Table S1, ESI†). Moreover, the remarkable effectiveness of SCD in stabilizing the Zn anode could increase the Zn utilization ratio. The symmetric cells with the ZS + SCD electrolyte using a thinner Zn anode (~9 μm, Fig. S31, ESI†) could still deliver a stable cycling lifespan of about 500 h at a high current density (5 mA cm^{-2}) and capacity (3 mA h cm^{-2}) with a depth of discharge (DOD) of 56.7%, while the cell with the ZS electrolyte could only work for 95 h (Fig. 4(k)). When the DOD was further increased to 68.5% and 80% under a higher current density of 10 mA cm^{-2} (with a Zn anode thickness of ~25 μm, Fig. S32, ESI†), the cycling lifespans of the symmetric cells were significantly prolonged (Fig. 4(l) and Fig. S33, ESI†), demonstrating the great potential of the ZS + SCD electrolyte for practical applications.

To illustrate the feasibility of the ZS + SCD electrolyte in practical use, Zn//$NH_4V_4O_{10}$ full cells were assembled. The SEM images and XRD patterns of the cathode material $NH_4V_4O_{10}$ are shown in Fig. S34–S37 (ESI†).[15,44] The CV curves of the full cells with the ZS and ZS + SCD electrolytes were recorded with a scan rate of 0.2 mV s^{-1} (Fig. 5(a)). Generally, the shape of the CV curve of the full cell with the ZS + SCD electrolyte was almost unchanged compared to that with the ZS electrolyte. Also, the comparable XRD patterns and XPS spectra of the discharged/charged cathode materials confirmed that SCD had negligible effect on the redox mechanism of $NH_4V_4O_{10}$ (Fig. S38 and S39, ESI†).[34] The CV curves at various scan rates were further collected to investigate the Zn^{2+}-storage process, and the b values were calculated based on the peak currents and scan rates as 0.85 and 0.57 for the cells without and with SCD, respectively (Fig. S40, ESI† and Fig. 5(b)).[45,46] The b values indicated that the cell using the ZS electrolyte showed a capacitive-dominant behavior, which could be altered to be diffusion-dominant with the addition of SCD (Fig. 5(c) and Fig. S41, ESI†). This was consistent with the reduced EDL capacitance and evidenced the promotional effect of SCD on Zn^{2+} diffusion. The improved electrochemical reaction kinetics could be attributed to the enhanced charge-transfer rate. The EIS spectra showed that the addition of SCD reduced the R_{ct} value of the full cells (Fig. S42, ESI†). Furthermore, the galvanostatic charge/discharge (GCD) profiles of the full cells with different electrolytes were recorded and the rate performance was evaluated at various current densities from 0.5 to 5 A g^{-1} (Fig. 5(d)–(f)). The lower polarizations (236.4 mV *vs.* 271.9 mV at 0.5 A g^{-1}) in the ZS + SCD electrolyte indicated its superior cycling stability (Fig. S43, ESI†).[47] The full cell using the ZS + SCD electrolyte only exhibited slightly higher specific capacities in the rate performance, which might have benefited from the optimized Zn^{2+}-deposition behavior as well as the reduced charge-transfer resistance. However, due to its impressive performance in stabilizing the Zn anode, the addition of SCD significantly improved the cycling stability of the full cells. Specifically, the full cell with the ZS + SCD electrolyte maintained a capacity of 282.6 mA h g^{-1} after 500 cycles at a current density of 1.0 A g^{-1} with a capacity retention of 80.3% (Fig. 5(g)). By contrast, the corresponding capacity and retention of the full cell with the ZS electrolyte was only 136.0 mA h g^{-1} and 37.3%. The promotion by SCD was also effective when the current density was elevated to 5 A g^{-1}, wherein the capacities of the full cells with and without SCD after 1500 cycles were 204.6 and 67.9 mA h g^{-1}, respectively (Fig. 5(h)). Clear microgrooves and irregular grains could be observed in the SEM images of the cycled Zn surface on the ZS surface, which were induced by the severe corrosion and undesirable deposition (Fig. S44a–c, ESI†). Meanwhile, most of the Zn deposition was in the form of large flakes, and the Zn surface was more even and flatter in the ZS + SCD electrolyte (Fig. S44d–f, ESI†). Simultaneously, the XRD patterns as well as EIS spectra for the cycled Zn surface also confirmed the equivalent efficacy of the protective effect of SCD in the full cells, which plays the dominant role in maintaining the stability and reversibility (Fig. S45 and S46, ESI†).[40,48] Furthermore, the assessment of the self-discharge and capacity retention behavior of the full cells was performed after the cells were fully charged to 1.6 V at 1.0 A g^{-1} and left standing for 48 h (Fig. 5(i) and (j)). The open circuit potential of the cell with the ZS + SCD electrolyte was stabilized at 1.0469 V with a CE of 88.1%, both of which were higher than the cell with the ZS electrolyte (1.0229 V and 85.5%), which was attributed to the effective inhibition of the side reactions by SCD. For practical application, Zn//$NH_4V_4O_{10}$ pouch cells were further assembled with the ZS + SCD electrolyte, which could provide a stable power supply for an LED light board

 This journal is © The Royal Society of Chemistry 2025

Published on 08 January 2025. Downloaded by BEIJING UNIVERSITY OF SCIENCE & TECHNOLOGY on 2/26/2025 2:41:04 PM.

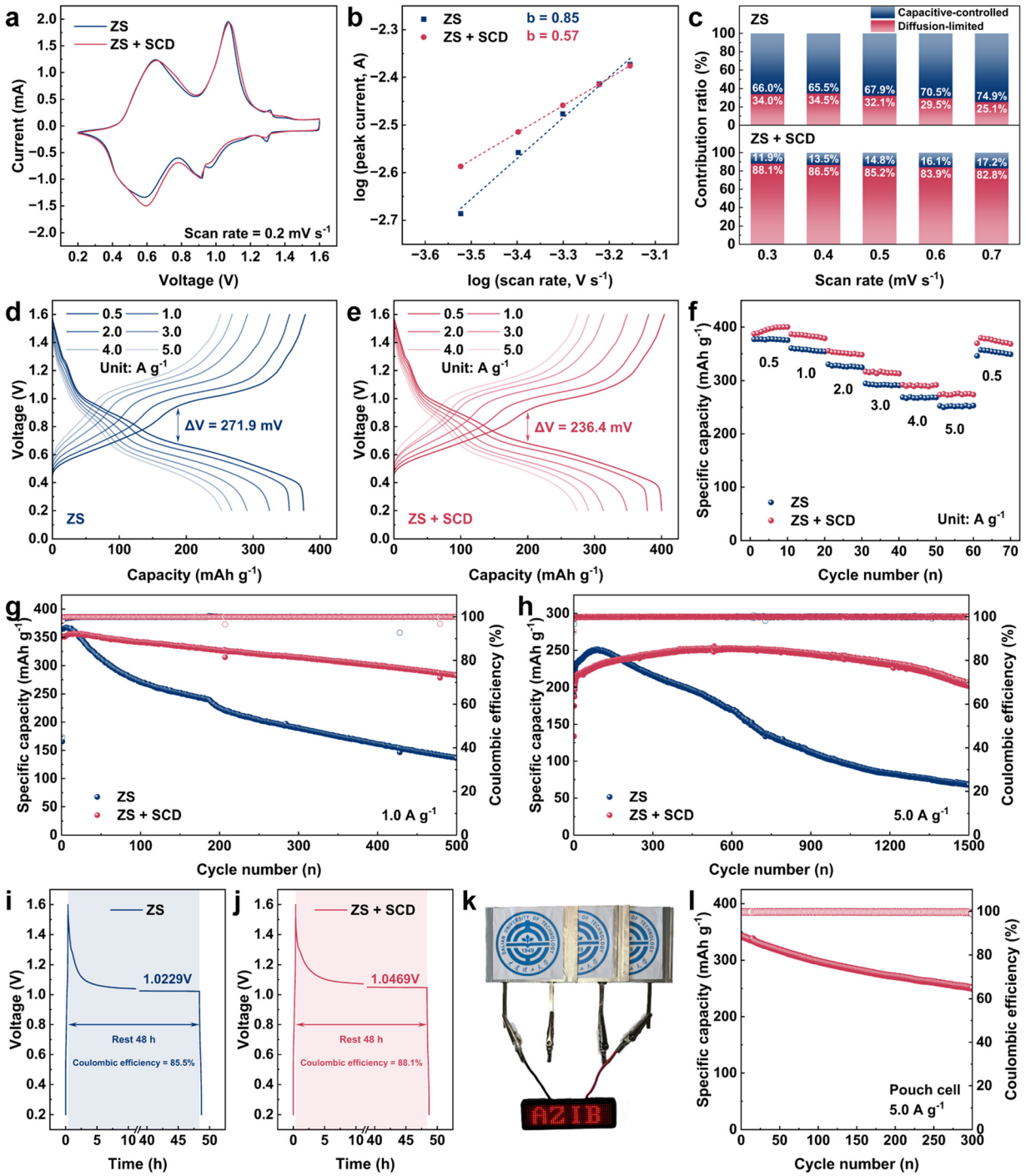

Fig. 5 (a) CV curves of the Zn//$NH_4V_4O_{10}$ full cells at 0.2 mV s^{-1}. (b) Fitting plots between log (*i*) and log (*v*) at different peak currents (c) contribution ratios of diffusion-limited and capacitive-controlled capacities at various scan rates. (d) and (e) Galvanostatic charge/discharge profiles at various current densities. (f) Rate performance and cycling performance at (g) 1 A g^{-1} and (h) 5 A g^{-1} of the Zn//$NH_4V_4O_{10}$ full cells using ZS and ZS + SCD electrolytes. (i) and (j) Capacity retention of the Zn//$NH_4V_4O_{10}$ full cells using ZS and ZS + SCD electrolytes. (k) Digital photograph of the pouch cells assembled using ZS + SCD electrolyte powering the LED board, and (l) corresponding long-term cycling performance at 5.0 A g^{-1}.

(Fig. 5(k)). The pouch cells could deliver a specific capacity of over 250 mA h g^{-1} after 300 cycles at 5.0 A g^{-1} (Fig. 5(l)), demonstrating the promising practical application potential of the ZS + SCD electrolyte in high-performance AZIBs.

3. Conclusion

In summary, we propose an effective electrolyte additive SCD with both abundant functional groups and beneficial structural features for high-performance AZIBs. Experimental characterizations and

Published on 08 January 2025. Downloaded by BEIJING UNIVERSITY OF SCIENCE & TECHNOLOGY on 2/26/2025 2:41:04 PM.

theoretical calculations demonstrated that the SCD could simultaneously stabilize the Zn surface and suppress the side reactions with multiple promotional effects: (1) the sulfonate groups can interact with Zn^{2+} to modulate the solvation structure; (2) the stronger affinity between the sulfonate groups and Zn surface can govern the specific adsorption configuration of SCD molecules, which can *in situ* construct two planes on the Zn surface with a progressively improved affinity to Zn^{2+} to drive the diffusion and uniform dispersion of Zn^{2+}; (3) the hydrophobic toroidal inner channel can facilitate the de-solvation process of Zn^{2+}. Consequently, the cycle life of a Zn//Cu asymmetric cell and Zn//Zn symmetric cell using the modified electrolytes could be significantly improved to over 3000 h and 3900 h (2 mA cm^{-2}, 1 mA h cm^{-2}), respectively. The symmetric cells further exhibited remarkable performance under high current densities with a high Zn utilization ratio. The corresponding Zn//$NH_4V_4O_{10}$ full cells delivered a higher specific capacity and better cycling stability than the cells using bare electrolytes, while the assembled pouch cells were also stable for over 300 cycles. This study highlights the importance and reveals the potential of combining the functional groups and structural features in the design of advanced electrolytes for the future practical development of high-performance AZIBs.

Author contributions

Miao Yu: conceptualization, investigation, methodology, funding acquisition, writing – original draft. Jiawei Mu: investigation. Lingfeng Wang: investigation, methodology. Yuchao Niu: visualization. Wenjie Si: investigation. Jiale Li: investigation. Xiaoyu Liu: investigation. Tiantian Li: funding acquisition, writing – review & editing. Xiangcun Li: funding acquisition, supervision, writing – review & editing. Wenji Zheng: funding acquisition, writing – review & editing. Yan Dai: funding acquisition, writing – review & editing. Xiaobin Jiang: funding acquisition, writing – review & editing. Gaohong He: funding acquisition, supervision, writing – review & editing.

Data availability

The data supporting this article have been included as part of the ESI.†

Conflicts of interest

There are no conflicts of interest to declare.

Acknowledgements

This work was financially supported by National Natural Science Foundation of China (22308047, 22021005, 22178041, 22208041); China Postdoctoral Science Foundation (2022M710580); Natural Science Foundation of Liaoning Province (2023-MS-353, 2023-MSBA-009); Fundamental Research Funds for the Central Universities (DUT22LAB603). The authors acknowledge the assistance of DUT Instrumental Analysis Center.

References

1 A. Innocenti, D. Bresser, J. Garche and S. Passerini, *Nat. Commun.*, 2024, **15**, 4068.
2 G. Zampardi and F. La Mantia, *Nat. Commun.*, 2022, **13**, 687.
3 D. Chao, W. Zhou, F. Xie, C. Ye, H. Li, M. Jaroniec and Q. Shi-Zhang, *Sci. Adv.*, 2020, **6**, eaba4098.
4 J. Cao, F. Zhao, W. Guan, X. Yang, Q. Zhao, L. Gao, X. Ren, G. Wu and A. Liu, *Small*, 2024, 2400221.
5 Y. Zhu, G. Liang, X. Cui, X. Liu, H. Zhong, C. Zhi and Y. Yang, *Energy Environ. Sci.*, 2024, **17**, 369–385.
6 Y. Zhou, X. Ni, B. Hao, X. Zhou, C. Yan, J. Zhou and T. Qian, *Energy Storage Mater.*, 2024, **66**, 103227.
7 X. Guo and G. He, *J. Mater. Chem. A*, 2023, **11**, 11987–12001.
8 H. Du, Z. Yi, H. Li, W. Lv, N. Hu, X. Zhang, W. Chen, Z. Wei, F. Shen and H. He, *Chem. – Eur. J.*, 2024, **30**, e202303461.
9 C. Yang, J. Xia, C. Cui, T. P. Pollard, J. Vatamanu, A. Faraone, J. A. Dura, M. Tyagi, A. Kattan, E. Thimsen, J. Xu, W. Song, E. Hu, X. Ji, S. Hou, X. Zhang, M. S. Ding, S. Hwang, D. Su, Y. Ren, X.-Q. Yang, H. Wang, O. Borodin and C. Wang, *Nat. Sustain.*, 2023, **6**, 325–335.
10 Q. Zhang, Y. Ma, Y. Lu, L. Li, F. Wan, K. Zhang and J. Chen, *Nat. Commun.*, 2020, **11**, 4463.
11 F. Bu, Y. Gao, W. Zhao, Q. Cao, Y. Deng, J. Chen, J. Pu, J. Yang, Y. Wang, N. Yang, T. Meng, X. Liu and C. Guan, *Angew. Chem., Int. Ed.*, 2024, **63**, e202318496.
12 H. Yu, D. Chen, X. Ni, P. Qing, C. Yan, W. Wei, J. Ma, X. Ji, Y. Chen and L. Chen, *Energy Environ. Sci.*, 2023, **16**, 2684–2695.
13 H. Dou, X. Wu, M. Xu, R. Feng, Q. Ma, D. Luo, K. Zong, X. Wang and Z. Chen, *Angew. Chem., Int. Ed.*, 2024, **63**, e202401974.
14 Z. Yang, Y. Sun, S. Deng, H. Tong, M. Wu, X. Nie, Y. Su, G. He, Y. Zhang, J. Li and G. Chai, *Energy Environ. Sci.*, 2024, **17**, 3443–3453.
15 K. Ouyang, S. Chen, W. Ling, M. Cui, Q. Ma, K. Zhang, P. Zhang and Y. Huang, *Angew. Chem., Int. Ed.*, 2023, **62**, e202311988.
16 K. Zhao, G. Fan, J. Liu, F. Liu, J. Li, X. Zhou, Y. Ni, M. Yu, Y.-M. Zhang, H. Su, Q. Liu and F. Cheng, *J. Am. Chem. Soc.*, 2022, **144**, 11129–11137.
17 R. Li, M. Li, Y. Chao, J. Guo, G. Xu, B. Li, Z. Liu, C. Yang and Y. Yu, *Energy Storage Mater.*, 2022, **46**, 605–612.
18 Y. Wang, S. Zhang, H. Wang, Y. Wang, Y. Liu, S. Dou, X. Miao, W. Deng, X. Lin and Q. Yuan, *J. Mater. Chem. A*, 2023, **11**, 17207–17216.
19 Y. Wang, B. Liang, J. Zhu, G. Li, Q. Li, R. Ye, J. Fan and C. Zhi, *Angew. Chem., Int. Ed.*, 2023, **62**, e202302583.
20 A. Zhou, H. Wang, X. Hu, F. Zhang, Y. Zhao, Z. Hu, Q. Zhang, Z. Song, Y. Huang, L. Li, F. Wu and R. Chen, *Sci. Bull.*, 2023, **68**, 2170–2179.
21 C. Meng, W. He, L. Jiang, Y. Huang, J. Zhang, H. Liu and J. J. Wang, *Adv. Funct. Mater.*, 2022, **32**, 2207732.
22 M. Qiu, P. Sun, Y. Wang, L. Ma, C. Zhi and W. Mai, *Angew. Chem., Int. Ed.*, 2022, **61**, e202210979.
23 Z. Liu, R. Wang, Y. Gao, S. Zhang, J. Wan, J. Mao, L. Zhang, H. Li, J. Hao, G. Li, L. Zhang and C. Zhang, *Adv. Funct. Mater.*, 2023, **33**, 2308463.

 This journal is © The Royal Society of Chemistry 2025

Published on 08 January 2025. Downloaded by BEIJING UNIVERSITY OF SCIENCE & TECHNOLOGY on 2/26/2025 2:41:04 PM.

24 R. K. Singh, K. Kunimatsu, K. Miyatake and T. Tsuneda, *Macromolecules*, 2016, **49**, 6621–6629.
25 J. Chen, N. Liu, W. Dong, Y. Xu, Y. Cao, S. Zhang, J. Hou, H. Bi, T. Lin and F. Q. Huang, *Adv. Funct. Mater.*, 2024, **34**, 2313925.
26 H. Wang, W. Ye, B. Yin, K. Wang, M. S. Riaz, B. B. Xie, Y. Zhong and Y. Hu, *Angew. Chem., Int. Ed.*, 2023, **62**, e202218872.
27 B. Wang, R. Zheng, W. Yang, X. Han, C. Hou, Q. Zhang, Y. Li, K. Li and H. Wang, *Adv. Funct. Mater.*, 2022, **32**, 2112693.
28 X. Yang, W. Li, Z. Chen, M. Tian, J. Peng, J. Luo, Y. Su, Y. Zou, G. Weng, Y. Shao, S. Dou and J. Sun, *Angew. Chem., Int. Ed.*, 2023, **62**, e202218454.
29 Y. Yang, Y. Li, Q. Zhu and B. Xu, *Adv. Funct. Mater.*, 2024, 2316371.
30 C. Huang, X. Zhao, S. Liu, Y. Hao, Q. Tang, A. Hu, Z. Liu and X. Chen, *Adv. Mater.*, 2021, **33**, 2100445.
31 Z. Liu, L. Ye, J. Xi, J. Wang and Z.-G. Feng, *Prog. Polym. Sci.*, 2021, **118**, 101408.
32 T. Li, S. Hu, C. Wang, D. Wang, M. Xu, C. Chang, X. Xu and C. Han, *Angew. Chem., Int. Ed.*, 2023, **62**, e202314883.
33 S. Chen, Y. Xia, R. Zeng, Z. Luo, X. Wu, X. Hu, J. Lu, G. Ehud, H. Pan, Z. Hong, Y. Mi, K. Tao and Y. Jiang, *Sci. Adv.*, 2024, **10**, eadn2265.
34 P. Li, J. Zhang, Y. Chen, L. Zhang, Z. Zhao and Z. Peng, *Adv. Funct. Mater.*, 2024, **34**, 2316605.
35 M. Yang, J. Zhu, S. Bi, R. Wang, H. Wang, F. Yue and Z. Niu, *Angew. Chem., Int. Ed.*, 2024, **63**, e202400337.
36 Z. Zhang, P. Wang, C. Wei, J. Feng, S. Xiong and B. Xi, *Angew. Chem., Int. Ed.*, 2024, **63**, e202402069.
37 T. Wei, L. e Mo, Y. Ren, H. Zhang, M. Wang, Y. He, P. Tan, Z. Li, W. Chen and L. Hu, *Energy Storage Mater.*, 2024, **70**, 103525.
38 K. Qiu, G. Ma, Y. Wang, M. Liu, M. Zhang, X. Li, X. Qu, W. Yuan, X. Nie and N. Zhang, *Adv. Funct. Mater.*, 2024, **34**, 2313358.
39 Y. Ding, L. Yin, T. Du, Y. Wang, Z. He, J. A. Yuwono, G. Li, J. Liu, S. Zhang, T. Yang and Z. Guo, *Adv. Funct. Mater.*, 2024, 2314388.
40 X. Liang, X. Chen, Z. Zhai, R. Huang, T. Yu and S. Yin, *Chem. Eng. J.*, 2024, **480**, 148040.
41 Y. Liu, X. Xu, M. Sadd, O. O. Kapitanova, V. A. Krivchenko, J. Ban, J. Wang, X. Jiao, Z. Song, J. Song, S. Xiong and A. Matic, *Adv. Sci.*, 2021, **8**, 2003301.
42 Y. Zuo, K. Wang, P. Pei, M. Wei, X. Liu, Y. Xiao and P. Zhang, *Mater. Today Energy*, 2021, **20**, 100692.
43 H. B. Chen, H. Meng, T. R. Zhang, Q. Ran, J. Liu, H. Shi, G. F. Han, T. H. Wang, Z. Wen, X. Y. Lang and Q. Jiang, *Angew. Chem., Int. Ed.*, 2024, **63**, e202402327.
44 J. Yin, M. Li, X. Feng, T. Cui, J. Chen, F. Li, M. Wang, Y. Cheng, S. Ding, X. Xu and J. Wang, *J. Mater. Chem. A*, 2024, **12**, 1543–1550.
45 J. Gong, J. Ying, X. Jia, R. Su, T. Zhao and H. Jiang, *Chem. Eng. J.*, 2024, **480**, 148267.
46 Q. Yan, Z. Hu, Z. Liu, F. Wu, Y. Zhao, R. Chen and L. Li, *Energy Storage Mater.*, 2024, **67**, 103299.
47 D. Li, T. Sun, T. Ma, W. Zhang, Q. Sun, M. Cheng, Z. Zha, W. Xie and Z. Tao, *Adv. Funct. Mater.*, 2024, 2405145.
48 H. Cao, X. Huang, Y. Li, Y. Liu, Q. Zheng, Y. Huo, R. Zhao, J. Zhao and D. Lin, *Chem. Eng. J.*, 2023, **455**, 140538.